



**SCIENTIFIC COUNCIL MEETING - JUNE 1998**

Hydrodynamics associated to the confluence of Labrador  
and North Atlantic currents over Flemish Cap in summer  
1997.

by

Julio Gil, Ricardo F. Sánchez, Marián Blanco and Ignacio  
Reguera

Instituto Español de Oceanografía, Promontorio de S.  
Martín s/n, P.O. Box 240, 39080 Santander, Spain;  
e-mail: julio.gil@st.ieo.es

**ABSTRACT**

This paper presents the results of the 1997 Flemish Cap physical oceanography survey. It was performed over 104 stations, being a low-pass filter ( $\lambda=60$  km) applied to the data in order to discern mesoscale structures, separated less than  $\lambda/2$  (30 km) from macroscale ones. The macroscale dynamic and related geostrophic velocity fields show anticyclonic circulation over the bank, although a relatively cyclonic vortex occurs over the eastern fringe of it. This is formed by cold waters, whereas warmer waters of uncertain origin whirl around the anticyclonic region, matching with the shallower part of the bank. The frontal area of convergence of both structures drafts a wave-like NW-SE flux across the bank. Quasigeostrophic Omega equation is also applied in order to assess the effects of vorticity advections in terms of vertical forcing and fertilization of upper levels of the water column.

**1. INTRODUCTION**

Flemish Cap is a ca. 200 km radius steep-sided plateau situated in NAFO division 3M, at about 47°N 45°W. Bathymetry ranges between 125 m on the central part and 700 m around the bank's edge. Characteristic slope is very steep at the southern half of the plateau, where 200 and 1000 m isobaths are just 20 nautic miles away, whereas this distance between isobaths increase gradually northwards. The ca. 1100 m deep Flemish Pass separates the Flemish Cap from the Grand Bank of Newfoundland, making an isolated bank of the former (Akenhead, 1982; Colbourne, 1997; Cerviño and Prego, 1997).

The general circulation of water masses is determined by the confluence of Labrador (hereafter on referred to as LC) and North Atlantic (hereafter on referred to as NAC) currents. The offshore branch of the LC follows the southward slope of the Grand Bank and, on getting to Flemish pass, its flow diverts around the Flemish Cap; a southward sub-branch flows through the Pass while the westward-induced other skirts the Bank around its north-northeastern slope. On a southwest-northeast direction, south of the Grand Bank, the Gulf Stream (hereafter on referred to as GS) circulates parallel to the 4000 m isobath. GS and LC merge there, resulting the formation of the subsequent NAC (Cerviño and Prego, 1997; Colbourne, 1997).

Over Flemish Cap, LC brings cold and less saline arctic waters (below 2°C and 34.3 PSU) which interact with the warmer and saltier north atlantic waters (above 12°C and 35.5 PSU). Water over Flemish Cap has usually been referred to as *mixed water* of LC and NAC (Hayes *et al.*, 1977; Anderson, 1984; Colbourne, 1997; Cerviño and Prego, 1997) although Akenhead (1986) postulates the northerly character of it, attributing its precedence mainly to LC and subsequent warming and readjustment dynamics. Dynamics of the frontal system associated to the confluence of warm and cold waters, is thought to dominate circulation dynamics on the region.

In summer, below a prominent thermocline, subsurface temperature minima have been reported in several papers (Karasyev, 1962; Templeman, 1974; Colbourne, 1993, 1995, 1996 and 1997; Cerviño and Prego, 1997). Its association to seasonal thermohaline fronts and emergence of LC is being discussed, as well as some sort of upwelling phenomena which have also been considered. The latter have been postulated after large spatial variation in water density has been found, although, as the work of Hayes *et al.* (1977) suggests, Flemish Cap is too deep to yield the typical wind-driven coastal upwelling.

Quasi-permanent residual anticyclonic circulation around the Flemish Cap is reported in most of previous studies (Kudlo *et al.*, 1984; Ross, 1981; and the review by Stein, 1996) although Hill (1973) found slightly reversed cyclonic movement around the bank at the time of sampling. Current features seem to yield poor flows over the Flemish Cap, as proven by Ross (1980). The anticyclonic vortex appears as a topographically induced gyre over the bank, as theoretically shown by some authors (Huppert, 1975; Huppert and Bryan, 1976) and experimentally by others (Taylor, 1923; Davis, 1972). Conditions for its formation are: high fluid stratification, conspicuous height of the topographical feature and weak flow (Huppert and Bryan, 1976).

Upon this basis, Kudlo *et al.* (1984) define at least four types of geostrophic flow depending on previously cited features and its variation with weather conditions. The anticyclonic gyre becomes predominant after quiescence of wind stress activity, whereas the passage of major storm events and associated wind forcing, breaks the stratification and contributes to the attenuation of the gyre and appearance of meandering flows across the bank or either a series of intermediate dynamical situations. The stability of the gyre eases ichthyoplankton retention over the shallower recruitment areas, being therefore seasonally-induced circulation relevant to egg and larvae drift away Flemish Cap. For instance, de Cárdenas and Gil (1994) by comparing circulatory patterns and egg distribution during different periods for which both data were available, observed certain situations favourable to the entrance of eggs from the exterior into the bank.

## 2. MATERIAL AND METHODS

The 1997 Flemish Cap physical oceanography survey was performed over 104 stations, paired to the majority of the 121 fish casts. The probe used was a Sea-bird® SBE 25, from Sea-bird electronics USA. It was configured to acquire data records at a rate of 2 per second. As the launching winch run at a speed of 1 meter per second, 2 data were stored per meter. The maximum depth ranged from 539 m at station E98 to 127 m at station E96.

Acquired data were processed with the SBE 25 supported software package (Seasoft® 4.203) in order to: discard warm-up data, average values per depth unit and convert them to ascii files. Selected variables were: pressure (dbars), salinity (PSU), temperature (deg. C) and sigma theta ( $\text{kg/m}^3$ ). A water column stabilization program was applied to the data, with the objective to smooth anomalous density distributions due to analytical errors.

Stations are homogeneously distributed over the study area, yielding a mean distance of 12 nautic miles one to each other (Fig. 1). This regular distribution allow us to apply an objective technique for detection of mesoscale structures similar to the one described by Tintoré *et al.* (1991.), Gil and Gomís (1994), Gil (1995) and Viúdez *et al.* (1996) A further successive analysis method to correct undesirable effects of inhomogeneous station data distribution (Buzzi *et al.*, 1991) was applied. The scale separation technique has been developed by Doswell (1977) and Maddox (1980), based on the filtering properties of the Barnes' objective analysis scheme (1964, 1973). A first analysis  $f_1$  operates as a low-pass filter and smooths the observed data field to define the macroscale. A second analysis,  $f_2$ , with cutoff located near the smaller resolvable scale is then carried out. The normalized difference between these two low-pass filters (a band-pass filter) is assumed to account for the mesoscale signal. The total field is recovered as the sum of the macroscale and the mesoscale contributions, the short wavelength noise being filtered by the analysis. Thus, besides the total analysis, independent analysis of each scale is also possible.

Dynamic calculations were based upon the dynamic topography field, which was calculated upon the 200 meters reference level; this level was the most adequate to embrace the vast majority of stations (only 13 stations were partially excluded). Then, the field of related parameters was constructed. Contour maps presenting the results were built with Surfer® 6.01. Isobaths are depicted as concentric discontinuous lines on all charts, the inner one representing the 170 m depth isoline. Line interval is 50 m.

### 3. RESULTS

#### Water masses over Flemish Cap

The chart of water temperature and salinity at 15 m (fig. 2a and 2b) has been drawn to show the original features of the various water masses as well as seasonal effects, e.g. spring-summer warming, of waters over Flemish Cap. Upon this basis, a distribution of the distinct water masses and their relation with dynamics referred on bibliography can be done.

Temperature chart at 15 m (fig. 2a) presents a typical summer-typed pattern. An stable structure over the shallower part of the bank, presumably geostrophically isolated, seems to have been warming during the summer. Surface water temperature values yield figures above 11° C (enclosed by the bold solid line in fig. 2a). On the contrary, fringing the plateau's northwestern slope intense influence of LC waters leaves conspicuous cold nuclei (below 10°C, dark in figure; minima of 7.6°C at station E40). Noticeable are also cold core nuclei around the eastern fringe of the bank. Their different haline properties, as will be discussed in next paragraph, suggest another source else than LC for their origin.

Salinity distribution at 15 m (fig. 2b) allows the characterization of the previously mentioned pattern to be assessed. It confirms the LC source of the northwestern cold nuclei, since they yield the lowest salinity values (below 33.1 PSU, dark in figure; minima of 32.7 and 32.9 PSU at E28, E29 and E37). LC supply and detachment of the eastern cold nuclei is to be questioned since they bear higher salinity figures (33.3-33.5 PSU) than those of the previously cited ones. These seem to have an origin else than LC waters, namely upwelling phenomena. The warm structure over the bank's shallower part show the highest figures of salinity (33.8 at E82 -163 m depth-). This confirms the put forward hypothesis that these are geostrophically isolated waters which have suffered from an acute effect of solar warming and subsequent evaporation, more than justifying causes to explain the salinity rise. This may be the anticyclonic gyre referred to in section 1. Elsewhere salinity ranges 33.1-33.4 PSU, presumably corresponding with a sort of modified LC water due to the front dynamics between and NAC and LC, hereafter on referred to as Typical Flemish Cap Waters (TFW).

#### Subsurface temperature minimum

As referred to as in the introduction, several authors describe the existence of subsurface temperature minima (hereafter on referred to as STM) in summer, below a prominent thermocline (Karasyev, 1962; Templeman, 1974; Colbourne, 1993, 1995, 1996 and 1997; Cerviño and Prego, 1997) after a sequence of stations in perpendicular N-S/W-E cross-bank transects were studied. The good and abundant distribution of stations of this survey and subsequent high resolution of the objective analysis techniques applied, as described in section 2, allow us to calculate the topography of the STM (fig. 3a) as well as associated SMT values (fig. 3b).

Over the northwestern fringe of Flemish Cap SMT's are clear and conspicuous, occurring at shallow depths, always below 50 m (fig. 3a, dark in figure). Prominent thermal inversions characterize stations distributed on this area. LC influences hydrographic features on this region. At the eastern part two shallow STM nuclei are also visible.

At the plateau's shallower part, over which warmer surface temperatures have been referred to, STM depth deepens uniformly down to 100 m and beyond. This is a clear sign of little influence of LC waters, and subsequent little mixing with those. Dynamical processes of the gyre's formation that put up homgeneization within the water column together with the summer warming causes both weakening and deepening of the STM's.

In fig. 3b, which presents the value of STM over Flemish Cap, an equal pattern to that previously described for SMT topography occurs, *i.e.* the colder the shallower SMT's. The northwestern area of the plateau joins the most conspicuous and colder SMT's (below 2.0°C, dark in the figure; minima of 0.0°C at station E15). Following the pattern described for surface water temperature in fig. 2a, the rest of SMT values are uniformly distributed between 3.0-3.5°C, corresponding with the type of water enclosed within the anticyclonic gyre. We therefore think that the existence of these SMT's is closely related to precise and fixed dynamical processes.

### Geostrophic circulation

Over Flemish Cap get fluxes with source in the eastern side of LC, that dip the plateau's northwestern fringe, as well as fluxes coming from the NAC dipping the southeastern part. Between these different water masses dynamical adjustment processes, upon the basis of the conservation of potential vorticity  $\Pi$ , occur. The theorem of conservation of potential vorticity:

$$D_H/D_t[(\zeta+f)/(H+\xi)] = 0, \text{ or}$$

$$D_H/D_t[\Pi] = 0$$

Where  $\zeta$  is relative vorticity,  $f$  the Coriolis parameter,  $H$  water depth and  $\xi$  the elevation of waterlevel above the mean surface. A decrease in ground bathymetry  $H$ , if not compensated by a sharp elevation of the surface  $\xi$ , will be accompanied by stretching of the vortex lines so that the system loses  $\zeta$  and  $\Pi$  remains therefore constant (Pedloski, 1987 pp39). That is exactly what causes that over Flemish Cap and centered on its shallower part the existence of the on literature and in section 1 referred anticyclone.

In this work, 200 m was to be reference level for the calculation of the geostrophic parameters. This level was the assumption that resembled with best accuracy the dynamical situation, and it was already used by Kudlo *et al.* (1984) for their calculations. 13 stations that did not reach the 200 m depth were extrapolated downward by appending below them the dynamic height profile of the nearest deeper station.

In fig. 4a vectors of geostrophic velocity from the *total field* of the dynamic topography at 10 m are represented for the study area. The most relevant feature is that, given the high resolution of the sampling strategy, a number of mesoscale and submesoscale both cyclonic and anticyclonic structures is ascertained. These are grouped within two main areas. One on the southwest a bold solid grey line encircles clockwise rotating structures whereas on the northwestern fringe second bold solid grey line marks anticlockwise rotating ones. Circulation elsewhere, namely northwestern region, is characterized by weak geostrophic flows.

This equilibrium status implies high variability and low stability of structures, and a number of adjustment processes are expected to occur. In order to obtain a low-noise picture, and as described in section 2, we have centered the band-pass response of the analysis filtering at a wavelength  $\lambda=60$  km, so that maximum-minimum structures separated less than  $\lambda/2$  (30 km) were smoothed. Results showing the macroscale of the dynamic topography at 10 m are presented in fig. 4b. Resulting structures show more stable features than for the total field, namely an anticyclone (dark in the figure) covering the majority of the bank, centered on the plateau's shallower part, and a cyclonic gyre on the northeastern fringe.

In figs. 2 (a and b) and 3 (a and b) it was shown that Flemish Cap's northwestern section was dipped by a surface intrusion of LC water. Yet cold, the low salinity values it bears no front is formed against the anticyclonic gyre's waters, since the latter contains warm but saltier water, resulting in smoothed and tiny horizontal density gradients. Therefore over the northwestern part of the bank, no dynamical structures associated to frontal areas and subsequent geostrophic adjustment are found (fig. 4b).

On the contrary, as previously said, over the north-northeastern fringe of the plateau, little influence of LC was found (figs. 2, a and b; figs. 3, a and b;), resulting in poor arctic features. Salinity of waters that meet over that spot is relatively higher than for LC waters, and similar to the waters lying over the centre of the bank. The high temperature difference between the waters associated to the cyclonic area and those in the centre of the bank gives as a result a density front. On the outer and eastern side there must exist an inner branch of the NAC which dips the slope of Flemish Cap from southwest to northeast, although the sampling strategy and distribution of stations does not allow us verify this hypothesis.

### Estimation of the vertical motion by the divergence of Q vector

The  $\omega$ -equation appears as the result of the combination of the quasi-geostrophic (QG) vorticity and thermodynamic equations. Using the classical notation (Pedloski, 1987):

$$(\partial/\partial t + \mathbf{v}_g \cdot \nabla_h) \zeta_g - (f/\rho_0) \cdot \partial/\partial z (\rho_0 w) = 0 \quad (1)$$

$$(\partial/\partial t + \mathbf{v}_g \cdot \nabla_h) \cdot (g/\rho_0) \cdot \rho' - N^2 w = 0 \quad (2)$$

Equation of the QG vorticity (1) tells us that ageostrophic vertical motions ( $w$ ), i.e. stretching or shrinking of the vortex lines, are consequence of geostrophic advection of potential vorticity ( $\zeta_g$ ) and changes in vorticity associated with the geostrophic motion. The thermodynamic equation (2) relates density variations and horizontal density advection with vertical velocity.

Thus the  $\omega$ -equation combines both concepts:

$$\frac{N^2 \nabla_h^2 w + f_0^2 \partial^2 w / \partial z^2}{A} = \frac{f_0 \partial / \partial z (\mathbf{v}_g \cdot \nabla_h \zeta_g)}{B} + \frac{(g/\rho_0) \nabla^2 (\mathbf{v}_g \cdot \nabla_h \rho')}{C} \quad (3)$$

In equation (3) term A expresses the vertical velocity, forced by terms B (vertical derivative of vorticity advection associated with the geostrophic current and C horizontal laplacian of advection of density (Tintoré et al., 1991).

Using this diagnostic equation, a qualitative reasoning about the vertical motion can be done. Since the  $\omega$ -equation is a Poisson-typed one, if  $w$  is sinusoidal in the three-dimensional space, when  $B + C < 0$ ,  $w$  in term A must be positive, i.e. upward motion (Tintoré et al., 1991). The signs criteria to be applied is: x positive to the east; y positive to the north and z positive upwards.

In a regime of strong meanders like our study area, term C becomes negligible in comparison to B. Under this assumption, and since geostrophic velocity  $\mathbf{V}_g$  decreases with depth, it implies that if in term B:

- $-\mathbf{v}_g \cdot \nabla_h \zeta_g < 0$ , it means negative vorticity advection, then  $w$  is negative (or bottomwards motion)
- $-\mathbf{v}_g \cdot \nabla_h \zeta_g > 0$ , it means positive vorticity advection, then  $w$  is positive (or upwards motion)

We have used the form of the omega equation introduced by Hoskins et al. (1978) where terms B+C appear as  $2\nabla\mathbf{Q}$  in the formulation of the, being:

$$\mathbf{Q} = g/\rho_0 [(\partial u_g / \partial x)(\partial \rho' / \partial x) + (\partial v_g / \partial x)(\partial \rho' / \partial y), (\partial u_g / \partial y)(\partial \rho' / \partial x) + (\partial v_g / \partial y)(\partial \rho' / \partial y)]$$

Thus, the diagnostic equation yields than if:

- $2\nabla\mathbf{Q} > 0$ , then  $w$  is negative (or bottomwards motion)
- $2\nabla\mathbf{Q} < 0$ , then  $w$  is positive (or upwards motion)

In fig. 5a relative geostrophic vorticity  $\zeta_g$  at 30 m is shown. Areas with positive and negative relative vorticity are associated with the different anticyclonic-cyclonic structures. Where the

meandering pattern associated to the flux around these anticyclonic-cyclonic structures is strong, the advective vorticity term becomes predominant. In consequence with omega equation in these areas vertical motions will be frequent, as shown in fig. 5b.

Anyway, the intensity of the vertical motions depends on the strength of the currents. In our case the current pattern in Flemish Cap are weak as previously stated. Therefore we think that the features associated to water masses must be related to their anticyclone-cyclonic structure better than the ageostrophic vertical dynamics.

#### Temperature by depth strata

Bathymetric aspects are important since the different water masses locate within layers depending on their density. Therefore each bathymetric strata will bear water with different characteristics.

In figs. 6 to 8 we show water temperature at different layers, corresponding with the main bathymetric strata of the bank. Thermal inversion causes deeper layers to bear slightly higher temperatures than the upper ones and, except in the southwestern area, temperature is quite uniform, ranging from 3.1 to 3.6°C. Temperature anomalies found in this southwestern area rise above 4.0°C. This may be due to sinking processes by convergent fluxes.

#### 4. REFERENCES

- Anderson, J.T. 1984. Early life history of redfish (*Sebastes spp.*) on Flemish Cap. *Can. J. Fish. Aquat. Sci.*, **41**(7): 1106-1116
- Akenhead, S.A. 1986. Water retention over Flemish Cap. The role of freshwater outflow in coastal marine ecosystems. *NATO ASI Series*, **G7**, 283-293. S. Skreslet ed.
- Barnes, S. L. 1964. A technique for maximizing details in numerical weather map analyses. *J. Appl. Meteor.*, **3**, 396-409.
- Barnes, S.L. 1973. Mesoscale objective map analysis using weighted time series observations. *NOAA Tech. Memo.* ERL NSSL-62, 60 pp. [NTIS COM-73-10781]
- Buzzi, A., D. Gomís, M.A. Pedder and S. Alonso. 1991. A method to reduce the adverse impact that inhomogeneous station distributions have on spatial interpolation. *Mon. Wea. Rev.*, **119**, 2465-2491
- Cárdenas, E. De and J. Gil. 1994. Geostrophic circulation and cod egg distribution in Flemish Cap. *Bol.Inst. Esp. Oceanogr.* **10**(2). 1994: 203-209
- Cerviño, S. and R. Prego, 1997. Hydrographic Conditions on the Flemish Cap in July 1996. *NAFO SCR Doc.*, **17**, Serial No. N2847
- Colbourne, E. 1993. Oceanographic conditions on the Flemish Cap during the summer of 1993, with comparisons to the Long-Term average. *NAFO SCR Doc.*, **93**, Serial No. N2300
- Colbourne, E. 1995. Oceanographic conditions on the Flemish Cap during the summer 1995, with comparisons to the 1961-1990 average. *NAFO SCR Doc.*, **102**, Serial No. N2625
- Colbourne, E. 1996. Oceanographic conditions on the Flemish Cap during the summer 1996, with comparisons to the previous year and the 1961-1990 average. *NAFO SCR Doc.*, **96**, Serial No. N2770
- Colbourne, E. 1997. Oceanographic conditions on the Flemish Cap during the summer of 1997, with comparisons to the previous year and the 1961-1990 average. *NAFO SCR Doc.*, **84**, Serial No. N2930

- Davis, P.A. 1972. Experiments on Taylor columns in rotating stratified fluid. *J. Fluid Mech.*, **54**, 691-717
- Doswell, C.A. III. 1977. Obtaining meteorologically significant surface divergence fields through the filtering property of objective analysis. *Mon. Wea. Rev.*, **105**, 885-892
- Gil, J. 1995. Inestabilidades, fenómenos de mesoescala y movimiento vertical a lo largo del borde sur del golfo de Vizcaya. *Bol.Inst. Esp. Oceanogr.* **11**(2). 1995: 141-159
- Gil, J. y D. Gomis 1994. Circulación geostrofica, dinámica de mesoescala y fertilización de los niveles superficiales en el sector norte del mar de Alborán. Julio de 1991. *Bol. Inst. Esp. Oceanogr.* **10** (1). 1994: 95-117.
- Hayes, R.M., D.G. Mountain and T.C. Wolford. MS 1977. Physical oceanography and the abiotic influence on cod recruitment in the Flemish Cap region. *ICNAF Res. Doc.* **54**, serial No. 5107, 33pp.
- Hoskins B.J., I. Draghici, H.C. Davies. 1978. A new look at the  $\omega$ -equation. *J. R. Met. Soc.*, **104**, 31-38
- Huppert, H.E. 1975. Some remarks on the initiation of inertial Taylor Columns. *J. Fluid Mech.*, **67**: 397-412
- Huppert, H.E. and K. Bryan. 1976. Topographically generated eddies. *Deep-sea Res.*, **23**: 655-679
- Karasayev, B.E. 1962. Hydrologic investigations carried out aboard the vessels of the Kaliningrad Council for People's Economy in 1961 in ICNAF Subareas 2 and 3. *ICNAF Res. Doc.*, **71**, Serial No. 1014, 10 pp.
- Kudlo, B.P., B.A. Borokov and N.G. Sapronevskaya. 1984. Waters circulation pattern on Flemish Cap from observations in 1977-82. *NAFO Sci. Coun. Studies*, **7**, 27-38
- Maddox, R.A. 1980. An objective technique for separating macroscale from mesoscale features in meteorological data. *Mon. Wea. Rev.*, **108**, 1108-1121
- Pedloski, J. 1987. *Geophysical Fluid Dynamics*. New York Inc. Springer-Verlag: 710 pp.
- Ross, C.K. 1980. Moored current meter data from Flemish Cap, January-July 1979. *NAFO SCR Doc.*, **106**, Serial No. N200
- Ross, C.K. 1981. The drift of satellite-tracked buoys on Flemish Cap, 1979-80. *NAFO Sci. Coun. Studies*, **1**: 47-50
- Stein, M. 1996. Flemish Cap – A review on Research Activities With Focus on Oceanographic Conditions. *NAFO Sci. Coun. Studies*, **25**: 1-24
- Taylor, G.I. 1923. Experiments on the motion of solid bodies in rotating fluids. *Proc. R. Soc. London, Ser. A*, **104**: 213-218
- Templeman, W. 1974. Temperature and salinities in the eastern Newfoundland area in 1973. *ICNAF Res. Doc.*, **71**, Serial No. 5104, 13 pp.
- Tintoré, J.; D. Gomis; S. Alonso and G. Parrilla. 1991. Mesoscale dynamics and vertical motion in the Alborán sea. *J. Phys. Oceanogr.* **21**: 811-823
- Viúdez, A., J. Tintoré, y R. Haney 1996. Circulation in the Alborán sea as determined by Quasi-Synoptic Hydrographic Observations. Part I: Three-Dimensional Structure of the Two Anticyclonic Eddies. *J. of Phys. Ocean.*, **26**, No. 5, 684-705.

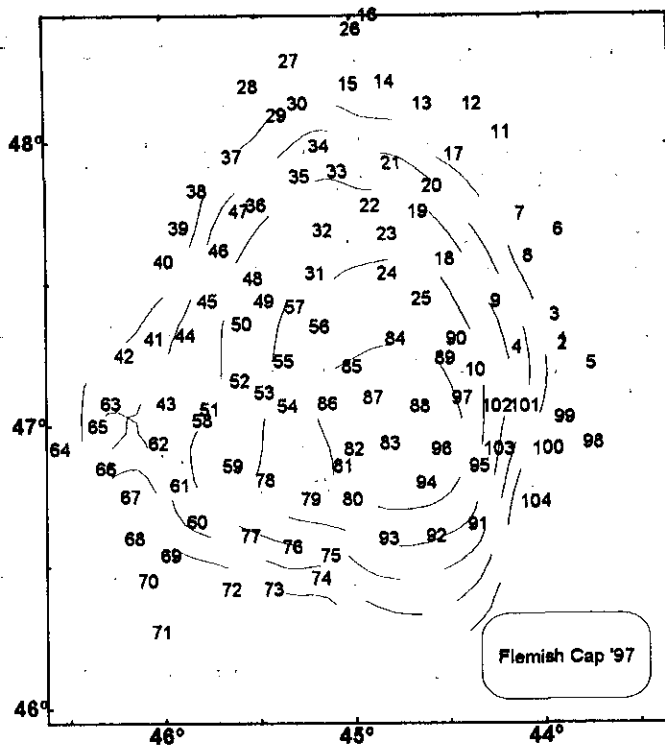
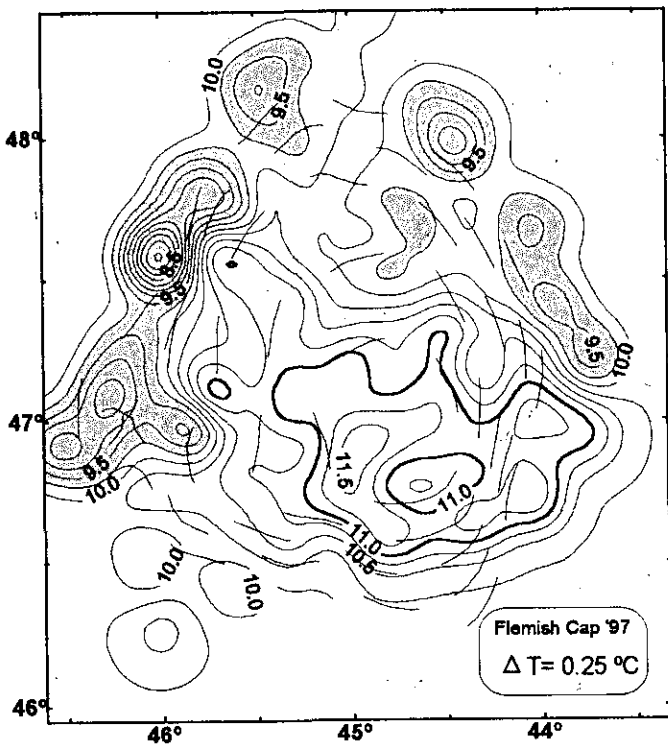
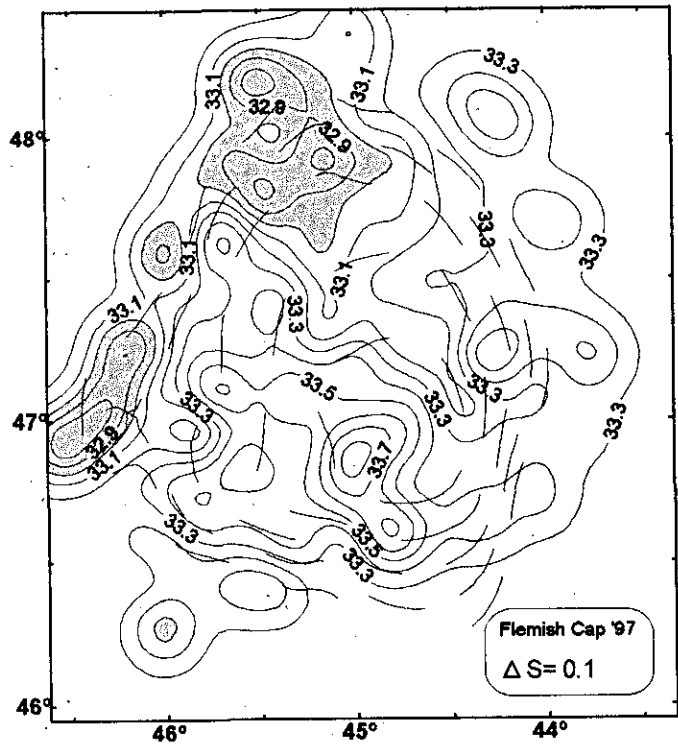


Figure 1. Sampling stations.



Temperature at 15 m ( $^\circ\text{C}$ )

Figure 2a. Temperature at 15 m



Salinity at 15 m (PSU)

Figure 2b. Salinity at 15 m

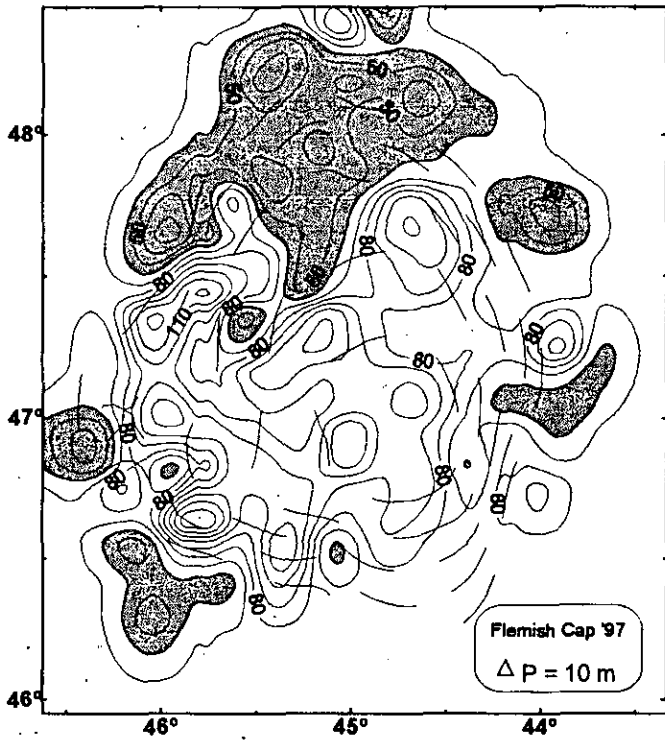


Figure 3a. Depth of Subsurface Temperature Minimum

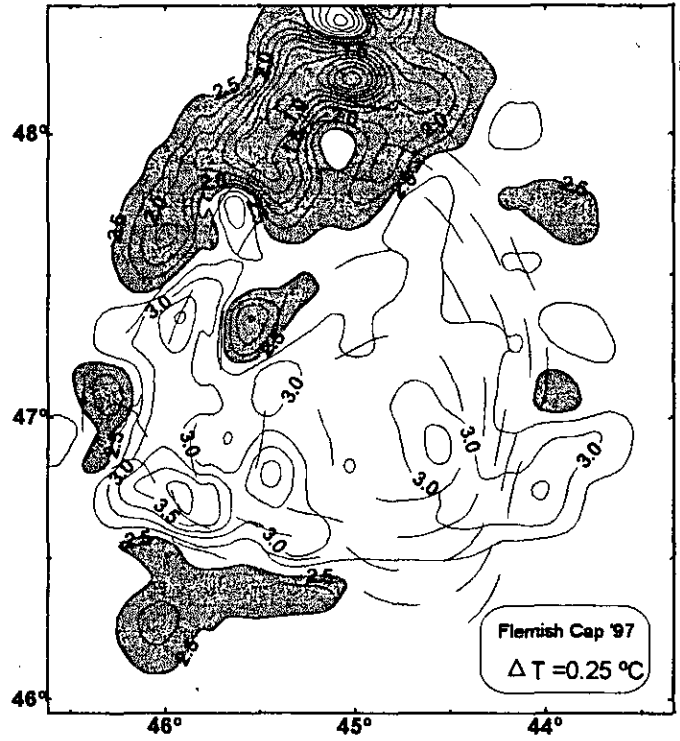


Figure 3b. Subsurface Temperature Minimum

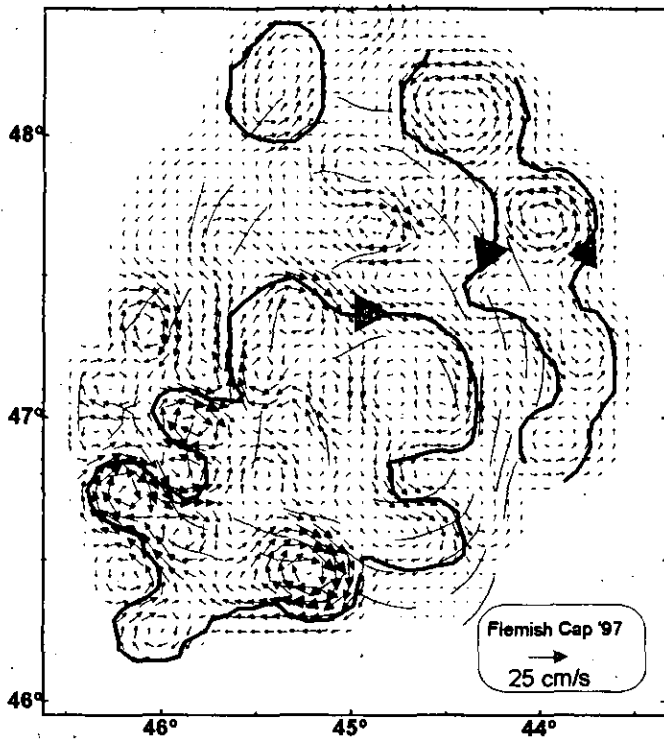


Figure 4a. Geostrophic current at 100 m ( $\text{cm}\cdot\text{s}^{-1}$ )

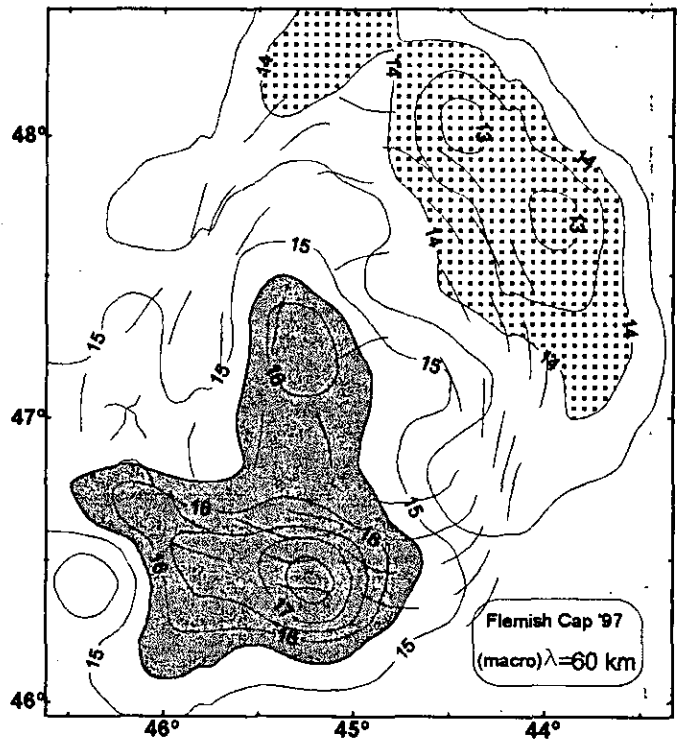


Figure 4b. Macroscale Dynamic Height ( $\lambda=60 \text{ Km}$ )

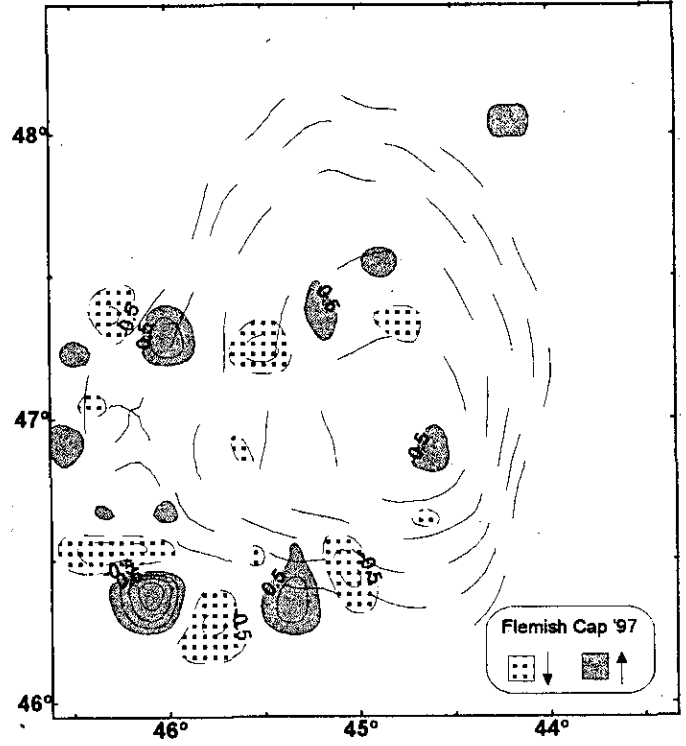
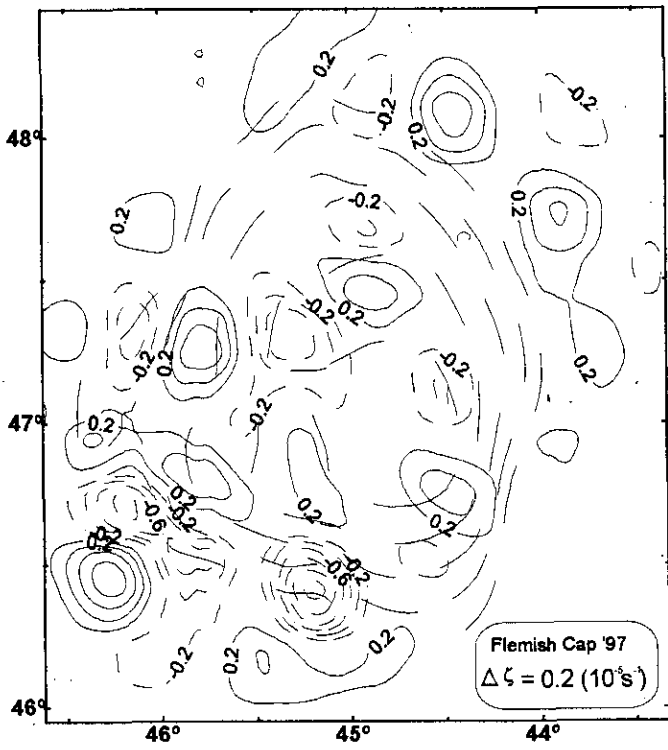
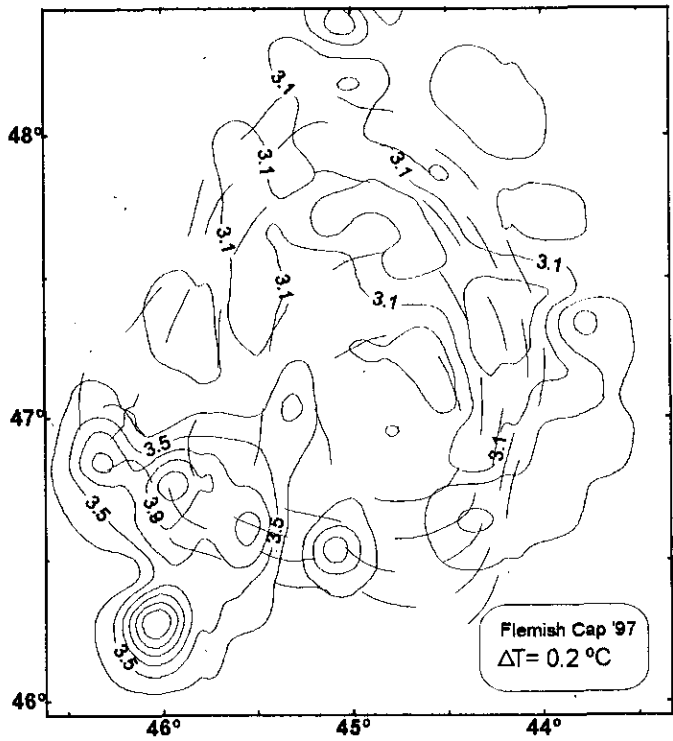
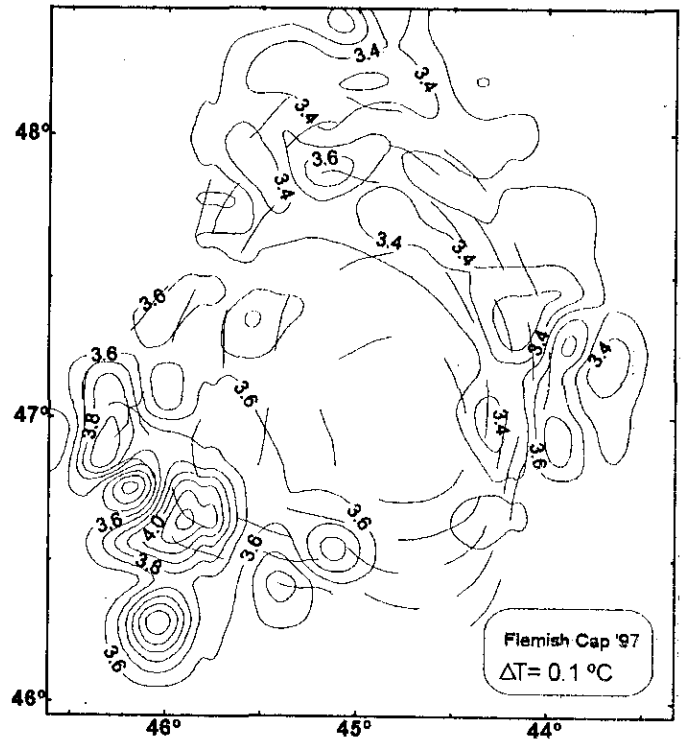


Figure 5a. Relative Geostrophic Vorticity ( $10^{-5} \cdot s^{-1}$ ) Figure 5b. Divergence of Q vector at 30 m ( $10^{-6} \cdot s^{-3} \cdot m^{-1}$ )



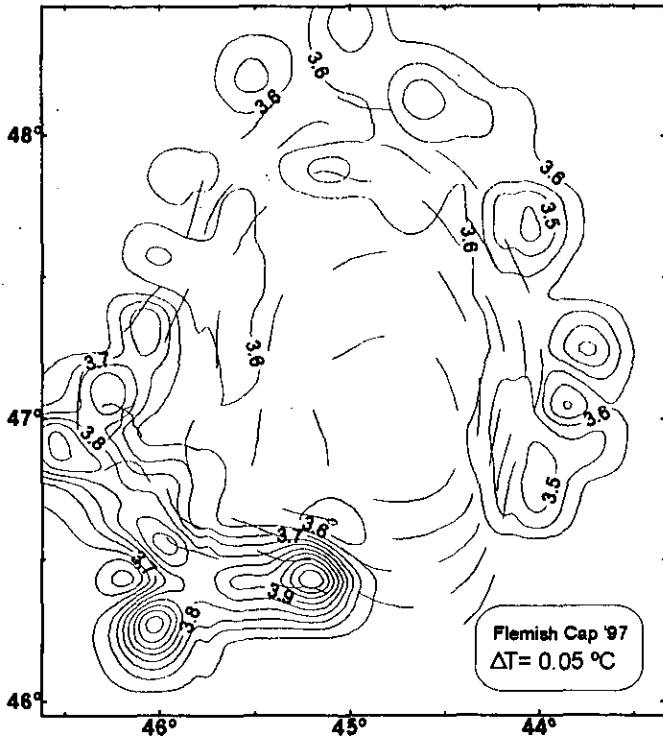
Temperature at 140 m (°C)

Figure 6a. Temperature at 140 m



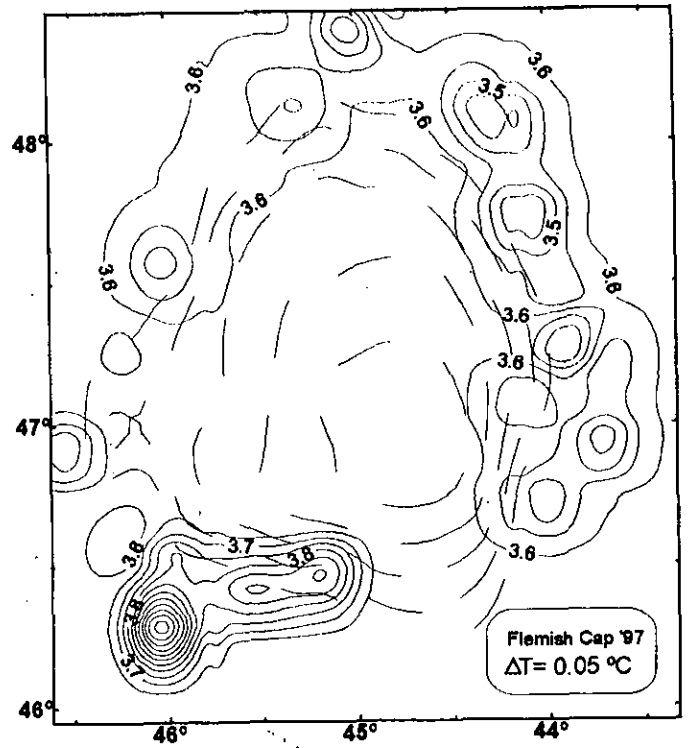
Temperature at 190 m (°C)

Figure 6b. Temperature at 190 m



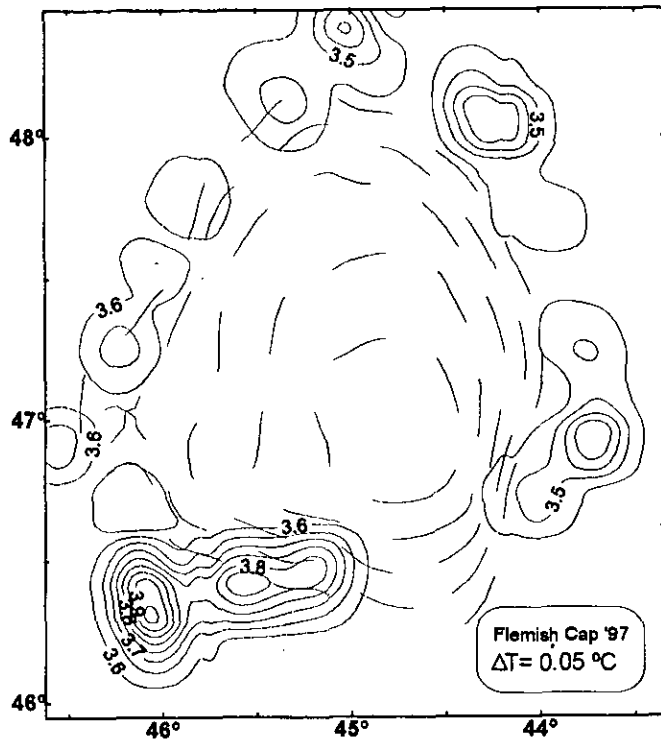
Temperature at 250 m (°C)

Figure 7a. Temperature at 250 m



Temperature at 300 m (°C)

Figure 7b. Temperature at 300 m



Temperature at 350 m (°C)

Figure 8. Temperature at 350 m